Rupatadine suppresses tumor growth and EMT in pancreatic cancer: Evidence from *in vitro* and *in vivo* models

BYUNG JO CHOI[1,2], HO JOONG CHOI[3], DOSANG LEE[2,3], JUNG HYUN PARK[2,4], TAE HO HONG[2,3], HEE-JUNG JUNG[5], GA-HEE JO[5], OK-HEE KIM[2,5] and SAY-JUNE KIM[2,3]

[1]Department of Surgery, Daejeon St. Mary's Hospital, College of Medicine, The Catholic University of Korea, Daejeon 34943, Republic of Korea; [2]Catholic Central Laboratory of Surgery, College of Medicine, The Catholic University of Korea, Seoul 06591, Republic of Korea; [3]Division of Hepatobiliary Pancreatic Surgery, Department of Surgery, Seoul St. Mary's Hospital, College of Medicine, The Catholic University of Korea, Seoul 06591, Republic of Korea; [4]Department of Surgery, Eunpyeong St. Mary's Hospital, College of Medicine, The Catholic University of Korea, Seoul 03312, Republic of Korea; [5]Translational Research Team, Surginex Co., Ltd., Seoul 06591, Republic of Korea

Received October 31, 2024; Accepted June 12, 2025

DOI: 10.3892/mmr.2025.13675

Abstract. Rupatadine, primarily used for treating allergic rhinitis as a selective histamine H1 receptor and platelet-activating factor antagonist, has potential anticancer properties, specifically through inducing lysosomal membrane permeabilization. The present study explores the efficacy of rupatadine in pancreatic cancer. The study assessed the effects of rupatadine on cell viability in AsPC-1 and MIA PaCa-2 pancreatic cancer cell lines at concentrations ranging from 0.001 to 50 μM. Additionally, a xenograft pancreatic cancer model in mice was used, with rupatadine administered intraperitoneally at 3 mg/kg three times weekly for 3 weeks. Tumor weights were measured 21 days post-treatment. Western blot analysis and immunohistochemical staining were conducted on excised tumor tissues to evaluate the impact on EMT and apoptosis. Rupatadine exhibited a concentration-dependent decrease in cell viability in both pancreatic cancer cell lines ($P<0.05$). *In vivo,* rupatadine significantly reduced tumor weight in the xenograft model compared with control groups ($P<0.05$). Further analysis revealed inhibition of EMT, evidenced by increased E-cadherin and decreased Vimentin and Snail levels. Apoptosis was enhanced, as shown by increased PARP and decreased Mcl-1 levels ($P<0.05$). Rupatadine shows significant anticancer potential in pancreatic cancer by inhibiting EMT and promoting apoptosis. These findings suggest that rupatadine could be developed as a novel therapeutic agent for pancreatic cancer, meriting further clinical investigation.

Correspondence to: Professor Say-June Kim, Division of Hepatobiliary Pancreatic Surgery, Department of Surgery, Seoul St. Mary's Hospital, College of Medicine, The Catholic University of Korea, 222 Banpo-daero, Seocho, Seoul 06591, Republic of Korea
E-mail: sayjunekim@catholic.ac.kr

Key words: anticancer therapy, apoptosis, epithelial-mesenchymal transition, pancreatic cancer, rupatadine

Introduction

Pancreatic cancer is known for its dire survival outcomes, with only about 12% of patients surviving beyond five years (1). This disease is expected to become the second leading cause of cancer-related deaths in the United States by 2040 (2). The late stage at diagnosis and high rate of recurrence after surgery significantly hinder long-term survival rates for those affected (3). Surgical resection is possible for merely 20% of these patients, as half of all cases are diagnosed after the cancer has metastasized to distant organs (4,5). Presently, the cornerstone of treatment for pancreatic cancer is combination therapy. This approach integrates traditional modalities like surgery, chemotherapy, and radiotherapy with more novel strategies such as immunotherapy and targeted therapy (6). Given this context, the development of novel anticancer agents with varied mechanisms of action is crucial to enhance the efficacy of combination therapy in treating pancreatic cancer.

Rupatadine, primarily known as a selective antagonist for the histamine H1 receptor and platelet-activating factor (PAF) for treating allergic rhinitis, has garnered attention for its potential anticancer effects (7-9). Its anticancer properties first stem from its ability to induce lysosomal membrane permeabilization, releasing lysosomal hydrolases into the cytoplasm, which damages mitochondria and initiates apoptosis. Further research has demonstrated Rupatadine's capability to disrupt the TGFβ1 signaling pathway, a critical promoter of cancer cell invasion, angiogenesis, and immune evasion within the tumor microenvironment, thus playing a significant role in hindering tumor progression and metastasis. Studies have shown that Rupatadine's influence on the TGF-β signaling pathway may also involve modulation of associated pathways such as PAF, NF-κB, and p65, thereby broadening its therapeutic potential (10-13).

Despite extensive research exploring Rupatadine as a potential anticancer agent across various cancer types (14-17), its specific impact on pancreatic cancer has not been thoroughly examined. This study is designed to rigorously assess Rupatadine's anticancer efficacy through comprehensive *in vitro* and *in vivo* experiments utilizing pancreatic cancer models. The principal aim of this study is to elucidate the molecular and cellular mechanisms by which Rupatadine influences pancreatic tumor cells. Furthermore, this research seeks to enhance our understanding of Rupatadine's pharmacological attributes and lay the groundwork for its potential clinical applications in oncology.

Materials and methods

Cell culture. The AsPC-1 (passage 11) and MIA PaCa-2 (passage 13) pancreatic cancer cell lines were obtained from the Korea Cell Line Bank (KCLB). KCLB routinely authenticates cell lines via short tandem repeat (STR) profiling to confirm their identity and screen for contamination. All cell lines were cultured under standard conditions and used at the specified passage numbers to ensure experimental consistency. Cultivation of AsPC-1 cells was conducted using Roswell Park Memorial Institute (RPMI) medium (Hyclone). Concurrently, MIA PaCa-2 cells were cultured in Dulbecco's modified Eagle's medium (DMEM)/High (Hyclone). Both media were enriched with a supplement comprising 10% fetal bovine serum (FBS; Hyclone), and 1% Penicillin-Streptomycin (Gibco BRL). The cell lines were incubated at a temperature of 37˚C in a humidified environment, with a 5% CO_2 atmosphere to ensure optimal growth conditions.

Cell viability assay. The assessment of cell viability for both AsPC-1 and MIA PaCa-2 cell lines was performed utilizing the Ez-cytox Cell Viability Assay Kit (Itsbio) according to the manufacturer's instructions. All experiments were performed in triplicate (n=3) to ensure reproducibility and statistical significance.

Western blot analysis. Lysis of AsPC-1and MIA PaCa-2 cells, as well as mouse tissue samples, was carried out using the EzRIPA Lysis kit (ATTO Corporation). Protein concentration was determined using the Bradford assay reagent (Bio-Rad). For protein visualization, Western blot analysis was performed using primary antibodies at a 1:1,000 dilution, obtained from Cell Signaling Technology. This was followed by incubation with horseradish peroxidase (HRP)-conjugated secondary antibodies at a 1:2,000 dilution, sourced from Vector Laboratories. Detection of specific immune complexes was achieved using the Western Blotting Plus Chemiluminescence Reagent (Millipore). The primary antibodies used targeted hPARP (Cell Signaling Technology, #9542), MCL-1 (Cell Signaling Technology, #5453), cleaved-caspase-3 (Cell Signaling Technology, #9664), TGF-βR1 (Abcam, ab31013), p-SMAD2/3 (Cell Signaling Technology, #8828s), SMAD2/3 (Cell Signaling Technology, #5678s), human E-cadherin (Abcam, ab76055), Vimentin (Abcam, ab92547), Snail, (Cell Signaling Technology, #3879), PUMA (Cell Signaling Technology, #98672), and β-actin (Sigma-Aldrich, A5541). All experiments were performed in triplicate (n=3) to ensure reproducibility and statistical significance.

Immunocytochemistry analysis. AsPC-1and MIA PaCa-2 were seeded into 8-well plate (SPL Life Science) at the concentration of 8,000 cells/well. After cultured overnight, the cells were fixed with 4% paraformaldehyde at room temperature for 10 min. Then the cells were blocked with incubation buffer (Normal Hores serum in PBS) for 1 h at room temperature. Following that, the cells were also stained with above antibodies and incubated at 4˚C protected from light. After 1 h incubation, the cells were washed twice and stained with 100 ng/ml DAPI for 10 min at room temperature. The immunocytochemistry staining utilized antibodies against E-cadherin (Santa Cruze Biotechnology, sc-8426), Vimentin (Santa Cruze Biotechnology, sc-373717), Snail (Genetex, GTX125918) and GAPDH (Santa Cruze Biotechnology, sc-365062). The final observation of the samples was conducted using a fluorescence imaging system (EVOS U5000; Invitrogen; Thermo Fisher Scientific, Inc.). All experiments were performed in triplicate (n=3) to ensure reproducibility and statistical significance.

Immunohistochemical analysis. For the immunohistochemical analysis, tissue sections that were formalin-fixed and paraffin-embedded underwent deparaffinization, followed by a rehydration process using a series of ethanol solutions. Epitope retrieval was then carried out in accordance with standard methodologies. The immunohistochemical staining utilized antibodies against BIM (Cell Signaling Technology, #2933s), Mcl-1 (Santa Cruze Biotechnology, sc-377487), E-cadherin (Santa Cruze Biotechnology, sc-8426), and Snail (Genetex, GTX125918). Post-staining, the samples were analyzed for antibody expression using a laser-scanning microscope (Eclipse TE300; Nikon).

TUNEL assay. The detection of apoptosis in pancreatic cancer cells was carried out using TUNEL analysis, employing the In Situ Apoptosis Detection Kit (Takara Bio Inc.), with the protocol adhering to the manufacturer's instructions. In summary, the procedure involved incubating sample slides with 50 μl of TUNEL reaction mixture and TdT labeling reaction mix for a duration of 1 h at 37˚C, ensuring the environment was dark. Following the incubation, the slides were washed three times using phosphate-buffered saline (PBS). The final observation of the samples was conducted using a fluorescence imaging system (EVOS U5000; Invitrogen; Thermo Fisher Scientific, Inc.).

Wound healing assay. The AsPC-1 and MIA PaCa-2 cell lines were cultured in 6-well plates until they reached full confluence. Subsequently, the growth medium was substituted with serum-free media, and the cells underwent a 72-h incubation period. Post-incubation, the cell monolayers were mechanically disrupted to create a wound, followed by the application of a test agent (rupatadine). An exact region of the wound was imaged using phase-contrast microscopy prior to the administration of these agents. This same region was imaged again after a 72-h period. The area of the wound was quantitatively assessed using image analysis techniques, both initially and after the 72-h interval. The rate of wound closure was

calculated based on the change in wound area over time, using the formula: [(initial wound area-final wound area)/initial wound area] x100, to express this change as a percentage. All experiments were performed in triplicate (n=3) to ensure reproducibility and statistical significance.

Animals study design. Our animal study design involved five-week-old male BALB/c nude mice (Orient Bio). Our animal experiments were approved by the Institutional Animal Care and Use Committee (IACUC) of the Catholic University of Korea (approval No. CUMC-2022-0014-01) and were conducted in accordance with institutional and national guidelines for the care and use of laboratory animals. For the xenograft pancreatic cancer model, $1x10^6$ AsPC-1 cells were subcutaneously injected into the mice. In the evaluation of rupatadine's *in vivo* efficacy, mice were grouped randomly, with each group containing five mice. After two weeks post-implantation of the tumor model, the mice were treated with rupatadine (3 mg/kg) administered intraperitoneally, three times a week for three weeks. Twenty-one days after initial treatment, the animals were euthanized, and the tumors were surgically removed for subsequent analysis. Animals were euthanized using compressed carbon dioxide (CO_2) gas at a displacement rate of 30-70% of the chamber volume per minute for 2-3 min. Loss of consciousness was confirmed by observing lack of response and faded eye color, and death was verified by cessation of respiration, cardiac arrest, and pupil dilation. Throughout the experiment, animal health was monitored daily, and humane endpoints-such as weight loss >20%, severe lethargy, or ulceration-were predefined and strictly observed.

Regarding the establishment and monitoring of tumor formation before initiating Rupatadine treatment, tumors were allowed to reach a predetermined size, specifically a volume of 100 mm^3, confirmed through visual inspection before the commencement of drug administration. The endpoint for the study was matched based on the time-point rather than the stage, ensuring that all groups were assessed over the same duration post-treatment initiation.

Rupatadine pharmacokinetics in mouse plasma and tissues. Mice received an intravenous dose of 10 mg/kg rupatadine. Plasma samples were collected at intervals from 5 to 360 min and processed by mixing with four volumes of acetonitrile, followed by centrifugation. Tissue samples at 5 and 60 min were prepared similarly. Rupatadine concentrations were measured using high-performance liquid chromatography (HPLC) with a Waters Arc system, a C18 column, and a mobile phase of methanol and 0.3 M sodium acetate (pH 4.4) at a 20:80 ratio, with a flow rate of 1 ml/min. The retention time for rupatadine was 5 min.

Statistical analysis. Statistical analysis was performed using SPSS 11.0 (SPSS Inc.), with data presented as mean ± standard deviation (SD). Normality was assessed using the Shapiro-Wilk test. The Kruskal-Wallis test with Dunn's post hoc test was used for multiple-group comparisons, while the Mann-Whitney U test and Student's t-test were applied for nonparametric and normally distributed two-group comparisons, respectively. Statistical significance was set at $P<0.05$.

Results

In vitro anticancer effects of rupatadine. Rupatadine is a chemical compound characterized by a cationic amphiphilic structure, consisting of a hydrophobic ring system and a side chain with a cationic amine group (Fig. 1A). To further evaluate the dose-dependent effects of rupatadine, dose-response curves were generated for AsPC-1 and MIA-PaCa-2 pancreatic cancer cells, as well as human pancreatic stellate cells (HPSC) (Fig. 1B). The IC50 values for AsPC-1 cells were 23.5 μM (24 h) and 24.9 μM (48 h), while for MIA-PaCa-2 cells, the IC50 values were 30.9 μM (24 h) and 35.1 μM (48 h). In the MIA-PACA cell line, rupatadine displayed lower cell viability compared to treatments with irinotecan (3.125-200 ng/ml), 5-fluorouracil (1-100 μM), and paclitaxel (1-10 nM) at both 24 and 48 h. This suggests that rupatadine may possess superior anticancer effects relative to these well-established chemotherapeutic agents (Fig. S1). In contrast, rupatadine exhibited significantly lower cytotoxicity in human pancreatic stellate cells (HPSC), with IC50 values of 66.8 μM at 24 h and 132.0 μM at 48 h, indicating a selectivity for pancreatic cancer cells over normal pancreatic cells. Data are presented as mean ± SD from three independent experiments. This data suggests that rupatadine preferentially inhibits pancreatic cancer cells while having a reduced effect on normal pancreatic cells.

Following the treatment with rupatadine, a concentration-dependent (0-25 μM) increase in the pro-apoptotic markers, PARP and cleaved caspase-3, and a decrease in the anti-apoptotic marker, Mcl-1, were observed in AsPC-1 pancreatic cancer cells, as evidenced by Western blot analysis ($P<0.05$) (Fig. 1C). A similar trend was noted in MIA PaCa-2 cells, demonstrating the compound's consistent apoptotic induction across different cell lines ($P<0.05$) (Fig. 1D). Data are presented as mean ± SD from three independent experiments. Additionally, Western blot analysis was employed to assess the impact of rupatadine on TGF-β signaling and EMT markers. The results indicate that Rupatadine significantly suppresses the expression of TGFβRI and diminishes the phosphorylated to total SMAD2/3 ratio in a dose-dependent manner in AsPC-1 cells ($P<0.05$) (Fig. 2A), implicating the inhibition of the TGFβ1 signaling pathway at the receptor level. The analysis further revealed that Rupatadine upregulated the epithelial marker E-cadherin while downregulating mesenchymal markers N-cadherin, Vimentin, and Snail, highlighting its role in thwarting EMT ($P<0.05$). Parallel results in MIA PaCa-2 cells reinforced rupatadine's efficacy in targeting both the TGFβ signaling pathway and EMT (Fig. 2B).

Effects of rupatadine on migration of pancreatic cancer cells. The impact of rupatadine on the migration of pancreatic cancer cells was evaluated using a wound healing assay. After creating a scratch in a confluent monolayer of AsPC-1 cells, the closure of the wound was monitored in response to increasing concentrations of rupatadine (0.01-25 μM). Increased concentrations of rupatadine, specifically at 25 μM, were correlated with a significant expansion of the scratch area, illustrating a dose-dependent suppression of cell migration in AsPC-1 cells (Fig. 3A). An analogous effect was recorded in MIA PaCa-2

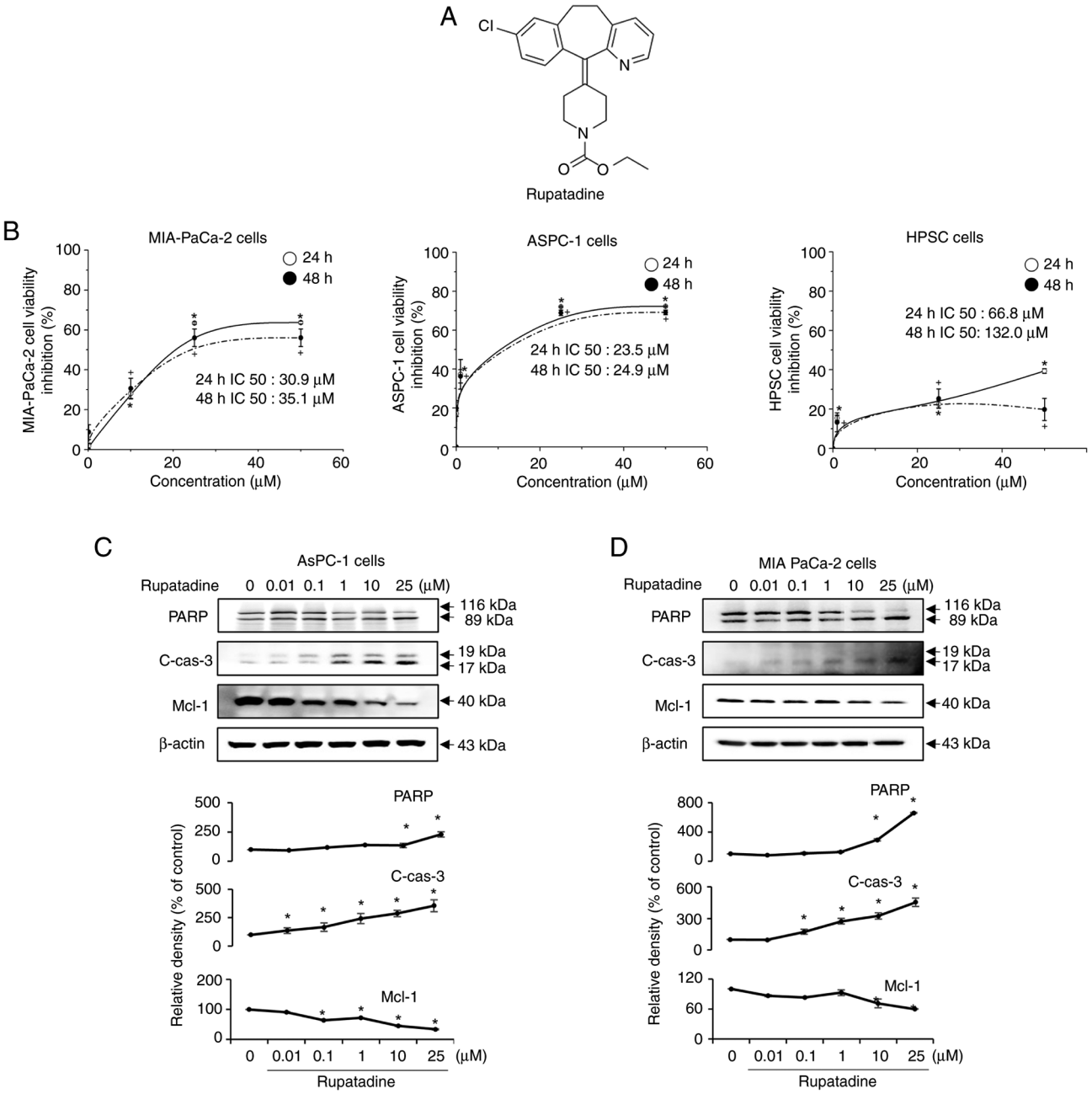

Figure 1. *In vitro* anticancer effects of rupatadine on pancreatic cancer cell lines. (A) Chemical structure of rupatadine. As a cationic amphiphilic drug, the structure of rupatadine, comprising a hydrophobic ring and a cationic amine group, facilitates its penetration through the plasma membrane. (B) Dose-response curves comparing the effects of rupatadine on AsPC-1 and MIA-PaCa-2 pancreatic cancer cells with those on HPSC (bottom). For the cancer cell lines, a dose-dependent decrease in viability is observed with rupatadine concentrations from 0 to 50 μM, with IC_{50} values of 23.5 μM (24 h) and 24.9 μM (48 h) for AsPC-1 cells (top, left) and 30.9 μM (24 h) and 35.1 μM (48 h) for MIA-PaCa-2 cells (top, right). By contrast, HPSCs (bottom) exhibit significantly higher IC_{50} values of 66.8 μM (24 h) and 132.0 μM (48 h), indicating lower sensitivity to rupatadine. (C) Induction of apoptosis in AsPC-1 cells. Western blot analysis shows a dose-dependent increase in the levels of pro-apoptotic markers PARP and cleaved caspase-3 and a reduction in the anti-apoptotic marker Mcl-1 in AsPC-1 pancreatic cancer cells following treatment with rupatadine, ranging from 0 to 25 μM ($P<0.05$). (D) Induction of apoptosis in MIA-PACA-2 cells. MIA-PACA-2 cells treated with rupatadine showed increased pro-apoptotic markers and decreased anti-apoptotic markers, similar to AsPC-1 cells, indicating rupatadine's consistent pro-apoptotic effect ($P<0.05$). Relative densities of individual markers had been quantified using Image J software and then were normalized to that of β-actin in each group. Values are presented as mean ± SD of three independent experiments. $^{*}P<0.05$ vs. the control after 24 h; $^{+}P<0.05$ vs. the control after 48 h. HPSC, human pancreatic stellate cells; Mcl-1, Myeloid cell leukemia-1; c-, cleaved; cas3, caspase 3.

cells at the 25 μM concentration of rupatadine (Fig. 3B). Data are presented as mean ± SD from three independent experiments.

Effects of rupatadine on EMT of pancreatic cancer cells. The influence of rupatadine on EMT in AsPC-1 pancreatic cancer cells was investigated through immunofluorescence analysis of EMT markers following treatment with rupatadine. Increasing the concentration of rupatadine (0.1-10 μM) resulted in a concentration-dependent increase in the immunofluorescence of the epithelial marker E-cadherin, and a decrease in the immunofluorescence of mesenchymal markers

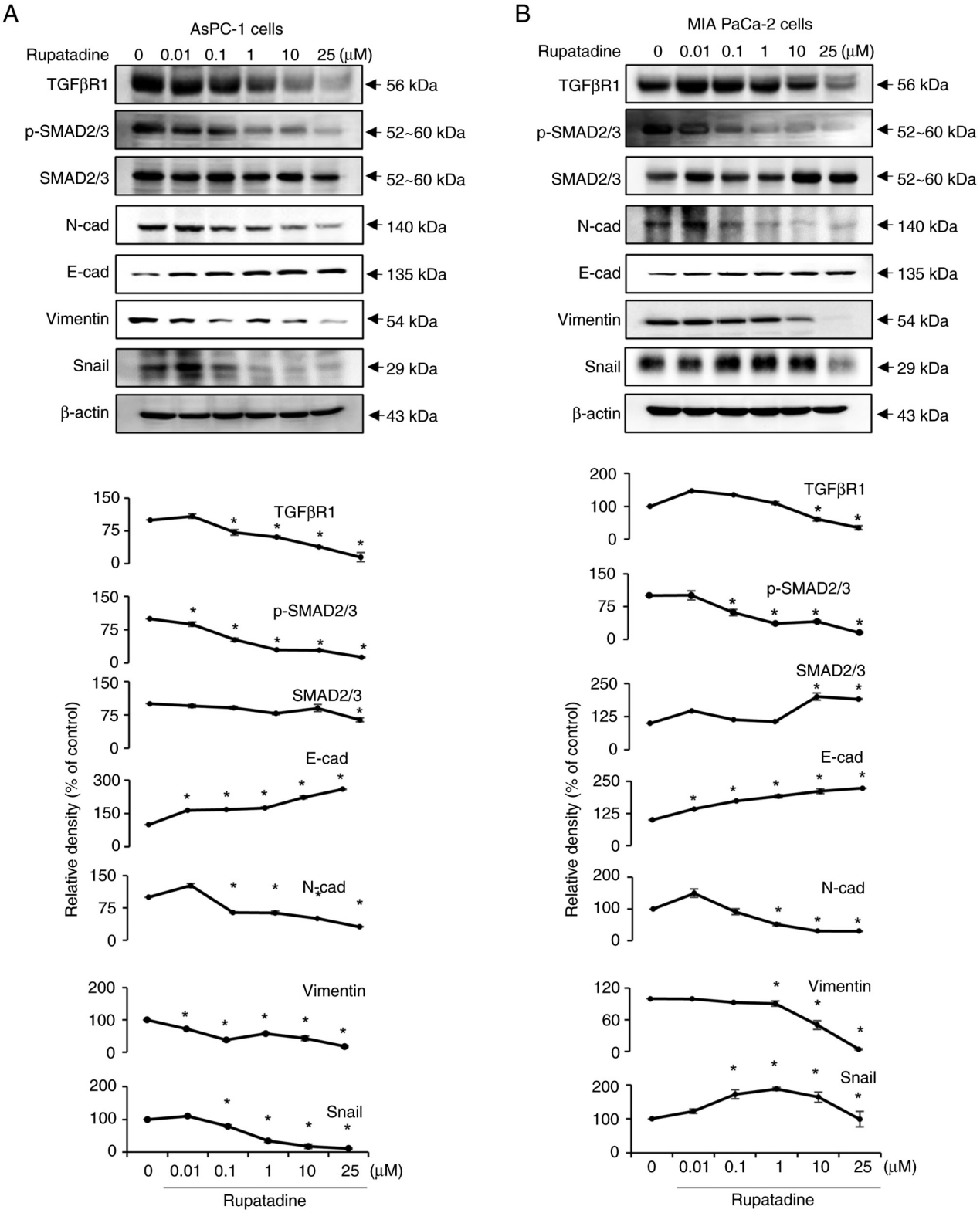

Figure 2. Effects of rupatadine on TGF-β signaling and EMT marker regulation. (A) In AsPC-1 pancreatic cancer cells, rupatadine exhibits a dose-dependent decrease in TGF-βRI expression and reduces the ratio of p-SMAD2/3 to total SMAD2/3, suggesting an inhibition of the TGFβ1 pathway. (B) In MIA PaCa-2 cells, analogous dose-dependent effects of rupatadine are observed, consistent with findings in AsPC-1 cells, further validating the drug's role in modulating TGF-β signaling and EMT. Relative densities of individual markers had been quantified using Image J software and then were normalized to that of β-actin in each group. Values are presented as mean ± SD of three independent experiments. *P<0.05 vs. the control. EMT, epithelial-mesenchymal transition; TGF-βRI, transforming growth factor β receptor type I; p-, phosphorylated; N-cad, N-cadherin; E-cad, E-cadherin.

Snail and Vimentin (P<0.05) (Fig. 4A). Similar effects were observed in MIA PaCa-2 pancreatic cancer cells, with rupatadine treatment leading to an increased immunofluorescence in E-cadherin and a decreased immunofluorescence in Snail and Vimentin (P<0.05) (Fig. 4B). Data are presented as mean ± SD from three independent experiments.

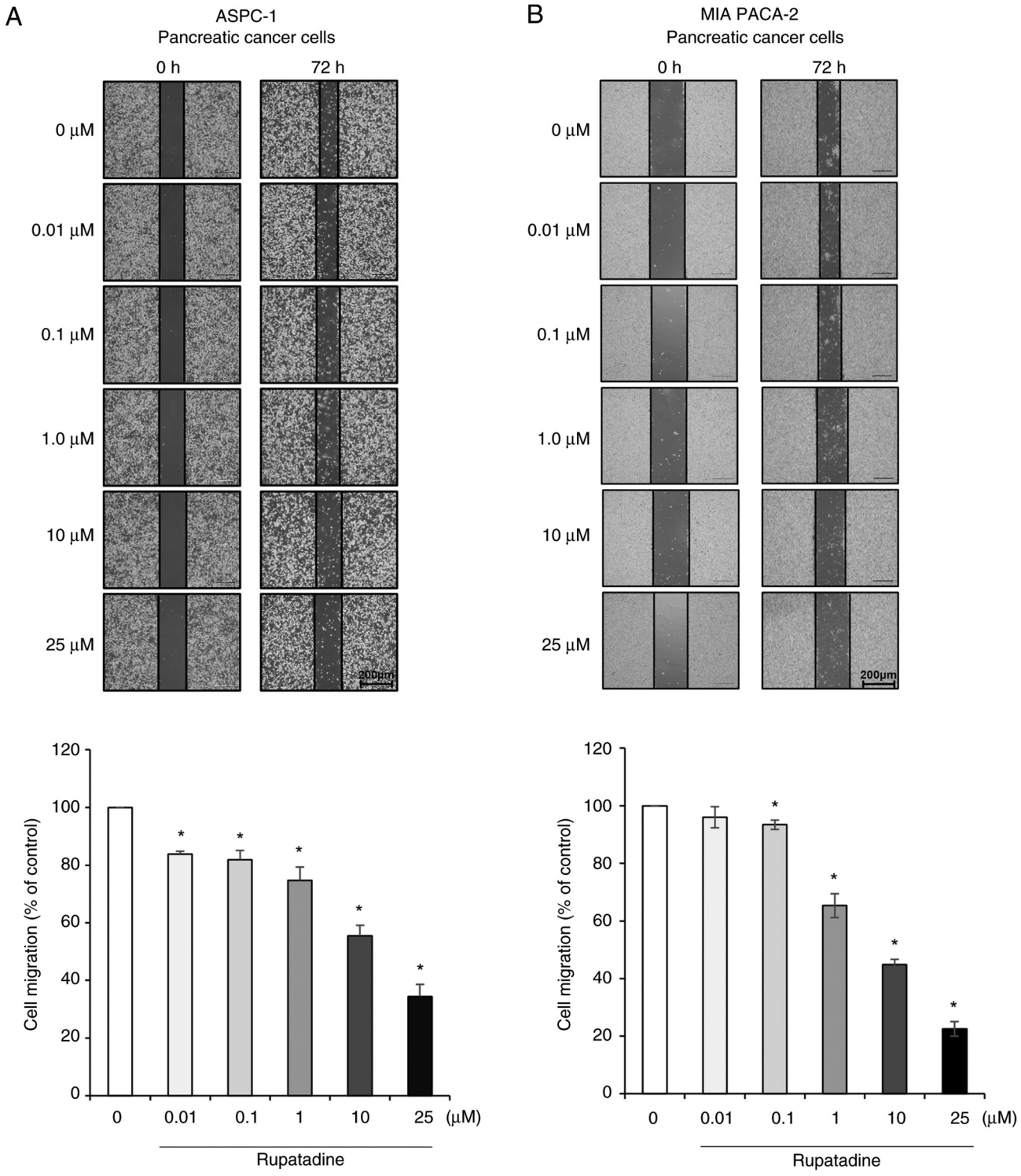

Figure 3. Impact of rupatadine on the migration of pancreatic cancer cells. (A) Wound healing assay in AsPC-1 cells. The assay involved monitoring wound closure in a monolayer of AsPC-1 cells, scratched and then treated with varying concentrations of rupatadine (0.01-25 μM). Results showed that higher concentrations of rupatadine significantly expanded the scratch area, indicating reduced cell migration. (B) Wound healing assay in MIA PaCa2 cells. Similar patterns to AsPC-1 cells were observed. Values are presented as mean ± SD of three independent experiments. Scale bar, 200 μm. *P<0.05 vs. the control.

Anticancer efficacy of rupatadine in a pancreatic cancer xenograft mouse model. The *in vivo* xenograft mouse model of pancreatic cancer was established by direct injection of AsPC-1 cells (1x10^6 cells) into the pancreas of BALB/c nude mice after laparotomy under anesthesia. Two weeks later, the mice were treated with rupatadine (3 mg/kg) administered intraperitoneally, three times a week for three weeks. On 21 days after initial treatment, the animals were euthanized, and the tumors were surgically removed for subsequent analysis. Fig. 5A presents a representative illustration depicting the difference in tumor size between the control group and the rupatadine-treated group on 21 days after initial treatment. Tumors in the control group weighed between 0.4 and 0.6 g, whereas those treated with Rupatadine weighed between 0.2

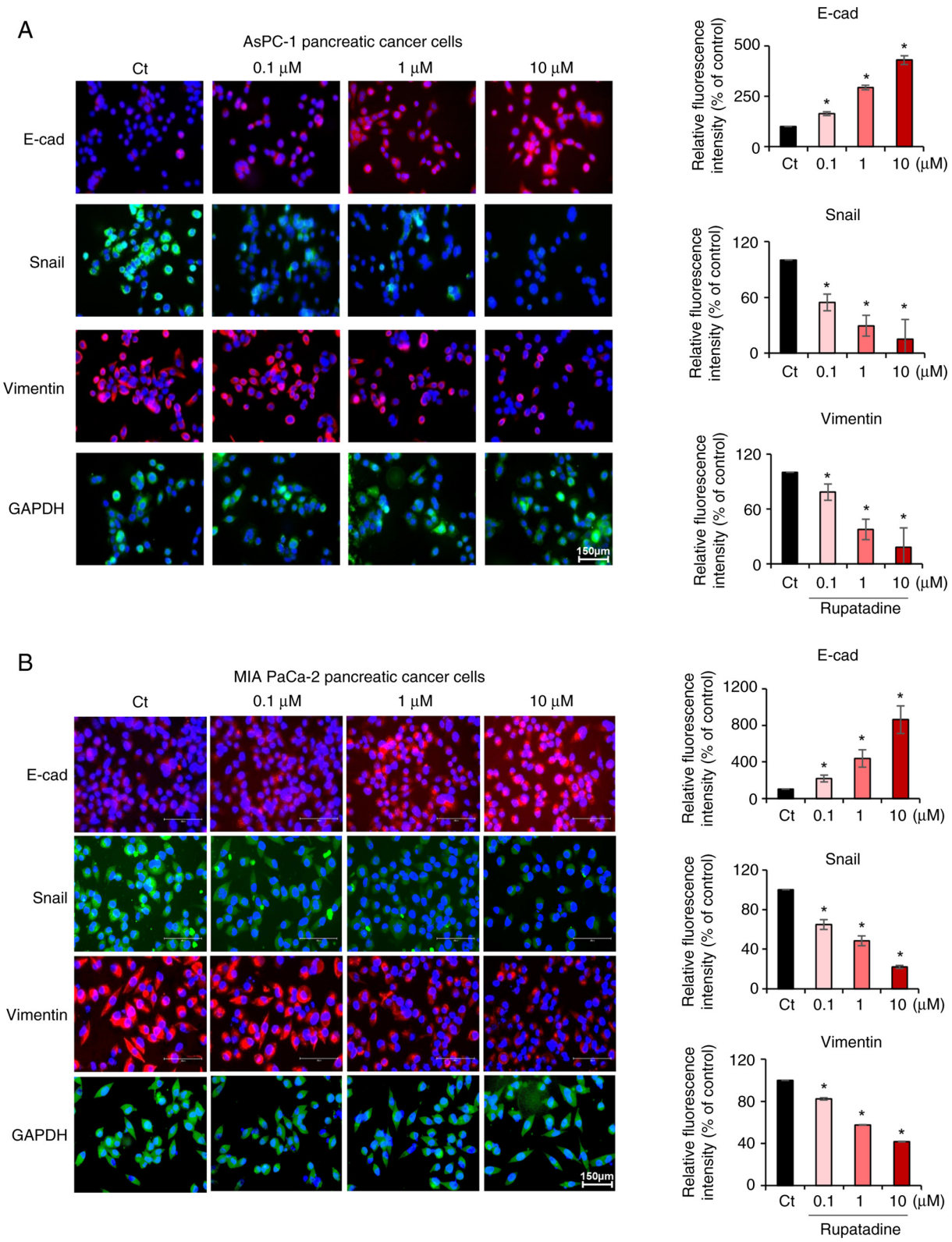

Figure 4. Immunofluorescence assay showing rupatadine's influence on EMT in pancreatic cancer cells. (A) Immunofluorescence in AsPC-1 cells. The assay revealed a dose-dependent increase in E-cadherin immunofluorescence and a decrease in Snail and Vimentin, indicative of EMT inhibition. (B) Immunofluorescence in MIA PaCa-2 cells. Similar patterns to AsPC-1 cells were observed. Values are presented as mean ± SD of three independent experiments. Percentages of immunoreactive areas were measured using NIH Image J and expressed as relative values to those in control tissues. Scale bar, 150 μm. *P<0.05 vs. the control. EMT, epithelial-mesenchymal transition; E-cad; E-cadherin; Ct, control.

and 0.3 g. To assess the effects of rupatadine on tumor progression over time, tumor volume was measured at multiple time points following treatment initiation. The rupatadine-treated group exhibited a significantly slower tumor growth rate compared to the control group (Fig. 5B top). After 21 days of treatment, the average tumor volume in the control

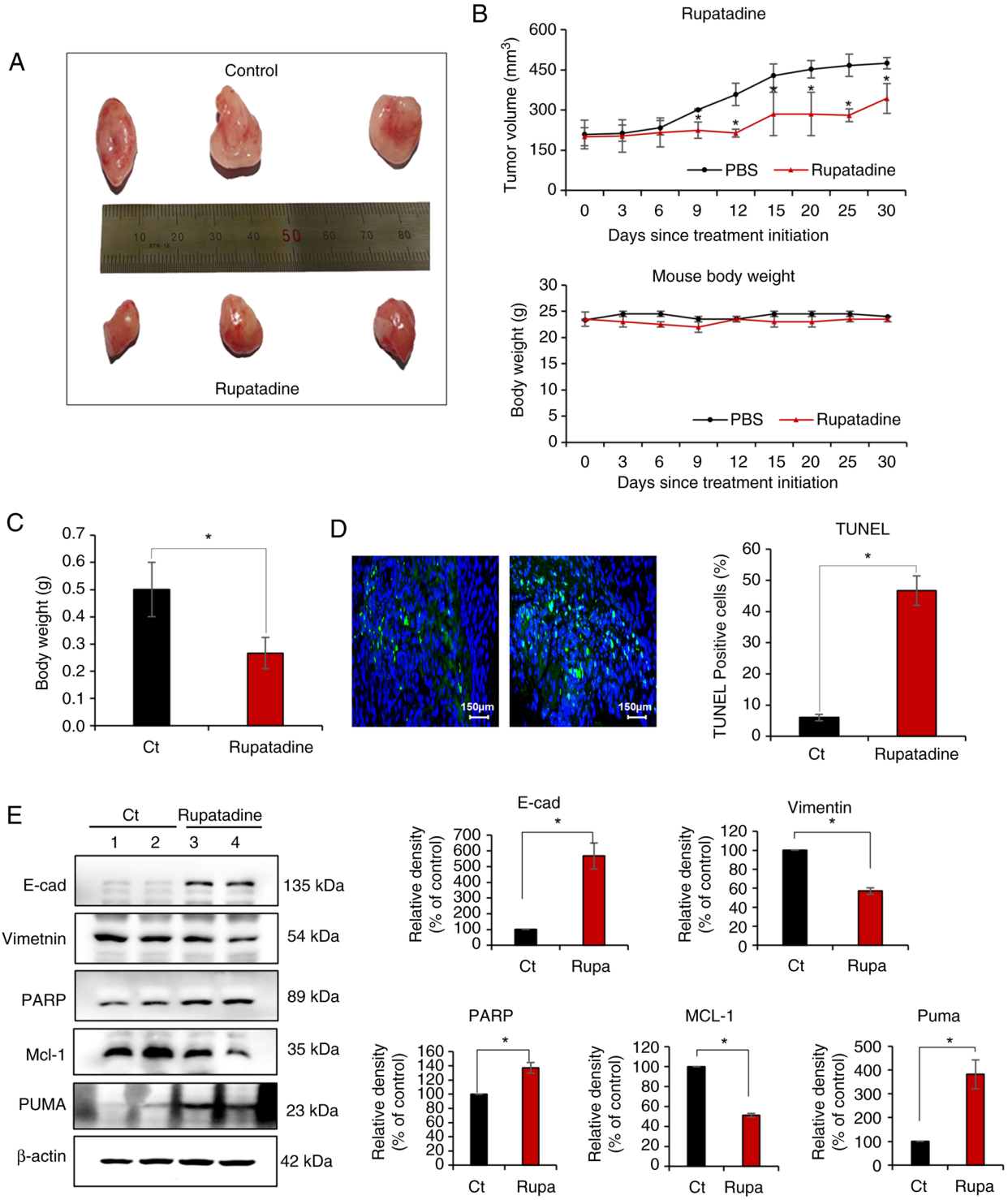

Figure 5. Anticancer efficacy of rupatadine in a pancreatic cancer xenograft mouse model. (A) Representative images of excised tumors from the control and rupatadine-treated groups on day 21 after initial treatment. (B) Tumor growth curve (top) showing a significantly slower tumor growth rate in the rupatadine-treated group compared to the control group. Body weight changes (bottom) indicate no significant differences between the groups, suggesting no systemic toxicity. (C) Tumor weight analysis on day 21 post-treatment, showing a significant reduction in the rupatadine-treated group ($P<0.05$). (D) TUNEL assay demonstrating a higher apoptosis index in the rupatadine-treated tumors compared to the control group ($P<0.05$). Scale bar, 150 μm (E) Western blot analysis of EMT and apoptosis-related markers in excised tumors. Rupatadine treatment increased E-cadherin and pro-apoptotic markers (PARP, PUMA) while reducing vimentin and the anti-apoptotic marker Mcl-1 ($P<0.05$). Relative densities of individual markers had been quantified using Image J software and then were normalized to that of β-actin in each group. Values are presented as mean ± SD of three independent experiments. *$P<0.05$ vs. the control. EMT, epithelial-mesenchymal transition; Mcl-1, Myeloid cell leukemia-1; E-cad; E-cadherin; Ct, control; PUMA, p53 upregulated modulator of apoptosis.

group continued to increase, whereas the tumor volume in the rupatadine-treated group showed a marked reduction (Fig. 5B top). In contrast, no significant differences in body weight were observed between the two groups throughout the experimental period, indicating that rupatadine treatment did not cause notable systemic toxicity (Fig. 5B bottom).

Consistently, tumor weight analysis performed on day 21 after the initial treatment revealed a significant reduction in the rupatadine-treated group compared to the control group ($P<0.05$), further supporting its tumor-suppressive effects (Fig. 5C). Data are presented as mean ± SD from three independent experiments.

Subsequently, a TUNEL assay was conducted to quantify apoptosis in the excised tumors from the rupatadine-treated groups. The results of the TUNEL assay revealed a significantly higher apoptosis index in the tumors treated with rupatadine compared to those in the control groups ($P<0.05$) (Fig. 5D). Western blot analysis was utilized to assess the differential expression of markers associated with EMT and apoptosis in the excised tumor tissues (Fig. 5E). In the group treated with rupatadine, a notable upregulation of the epithelial marker E-cadherin was observed, in contrast to the control group. Conversely, the mesenchymal marker vimentin was significantly downregulated ($P<0.05$) in the rupatadine-treated tumors. Furthermore, the rupatadine-treated tumors demonstrated a significant elevation in the levels of pro-apoptotic markers, PARP and PUMA, while the expression of the anti-apoptotic marker Mcl-1 was markedly reduced ($P<0.05$). Data are presented as mean ± SD from three independent experiments.

Effects of rupatadine on histological changes, apoptosis, EMT, and pharmacokinetics in a pancreatic cancer xenograft mouse model. Tumor tissues derived from a mouse xenograft model of pancreatic cancer underwent Hematoxylin and Eosin (H&E) staining for comparative histological examination. In the rupatadine-treated group, a notable reduction in tumor cell density was observed (Fig. 6A). This was followed by immunohistochemical staining of the excised tumor tissues from each experimental group. Analysis of the stained tissues revealed that, in the rupatadine-treated group, there was a significant increase in the percentage of immunoreactive areas for a pro-apoptotic marker, BIM, compared to the control group. Conversely, the expression of Mcl-1, an anti-apoptotic marker, was significantly decreased ($P<0.05$) (Fig. 6B top). Furthermore, the rupatadine-treated group exhibited a significant increase in the percentage of immunoreactive areas for the epithelial marker E-cadherin, alongside a significant decrease in Snail, a mesenchymal marker ($P<0.05$) (Fig. 6B bottom). Overall, these findings suggest that rupatadine treatment can attenuate the EMT process and enhance apoptosis in pancreatic cancer tissues within this mouse xenograft model.

To further investigate the *in vivo* pharmacokinetics of rupatadine, we analyzed its plasma concentration and tissue distribution following intravenous injection (10 mg/kg) in mice. Plasma concentration-time profiling demonstrated a rapid decline in rupatadine levels, with detectable concentrations at 5, 15, 30, and 60 min, but no detectable levels after 180 min, indicating fast clearance from circulation (Fig. 6C, left). Tissue distribution analysis revealed that rupatadine primarily accumulated in the liver and kidneys within 5 min post-injection but was largely undetectable in these tissues by 60 min, suggesting rapid metabolism and excretion (Fig. 6C, right). These findings provide essential information regarding rupatadine's pharmacokinetic profile and tissue clearance dynamics, which are critical for understanding its potential as an anticancer agent.

Discussion

Rupatadine, known for its role as a selective histamine H1 receptor and platelet-activating factor antagonist in treating allergic rhinitis, has gained attention for its anticancer potential due to its capacity to induce lysosomal membrane permeabilization. This research explores the anticancer properties of rupatadine within *in vitro* and *in vivo* pancreatic cancer models. Rupatadine demonstrated a concentration-dependent reduction in the cell viability of both AsPC-1 and MIA PaCa-2 pancreatic cells, across a range of concentrations (0.001-50 μM). In an *in vivo* pancreatic cancer xenograft model, intravenous administration of rupatadine led to a significant tumor weight reduction after 35 days of treatment. Further analysis of excised tumor tissues from the mouse model corroborated the *in vitro* findings, with rupatadine inhibiting EMT and promoting apoptosis in tumor cells. Specifically, it increased E-cadherin levels while decreasing Vimentin and Snail expressions, indicating a suppression of EMT. Concurrently, it augmented the expression of the pro-apoptotic marker PARP and reduced the anti-apoptotic marker Mcl-1, suggesting an enhancement of apoptotic pathways. Collectively, these findings underscore the potential of rupatadine as a therapeutic agent in pancreatic cancer due to its ability to concurrently inhibit EMT and activate apoptotic pathways in both *in vitro* and *in vivo* models of pancreatic cancer.

Rupatadine, widely used as an antagonist for histamine H1 receptors and platelet-activating factors in allergic rhinitis treatment, has garnered attention for its potential anticancer effects, particularly in acute myeloid leukemia (AML) and ovarian cancer (7,9). Specifically, research has shown that rupatadine affects AML cells at concentrations marginally higher than those used for alleviating allergic symptoms (9). In the study, rupatadine showed no substantial impact on the viability of normal blood cells, such as T cells, B cells, and myeloid cells, with the exception of a noted decrease in the myeloid cell population. Moreover, the treatment preserved the clonogenic capacity of healthy hematopoietic progenitor/stem cells, indicating a selective action against cancer cells while sparing healthy cells. Additionally, *in vivo* experiments demonstrated that rupatadine reduced the regeneration potential of AML cells when transplanted into immunocompromised mice, further supporting its potential as an anticancer agent. These findings highlight the potential of rupatadine as a selective treatment option for AML, revealing a new avenue for the use of this antihistamine beyond its traditional role in allergy management.

This study offers preliminary insights into rupatadine's ability to inhibit EMT, an effect not widely recognized in previous research. The inhibitory effect of rupatadine on EMT can reasonably be ascribed to its capacity to induce lysosomal membrane permeabilization and mitochondrial damage. This can lead to increased cellular stress, potentially disrupting EMT-related signaling pathways and modulating transcription factors crucial for EMT, such as Snail, Slug, and Twist. Additionally, rupatadine's impact on cellular stress and mitochondrial dysfunction could reduce the metastatic potential of cancer cells and alter autophagic flux, further contributing to the inhibition of EMT (9). These combined effects, stemming from rupatadine's disruption of lysosomal and mitochondrial

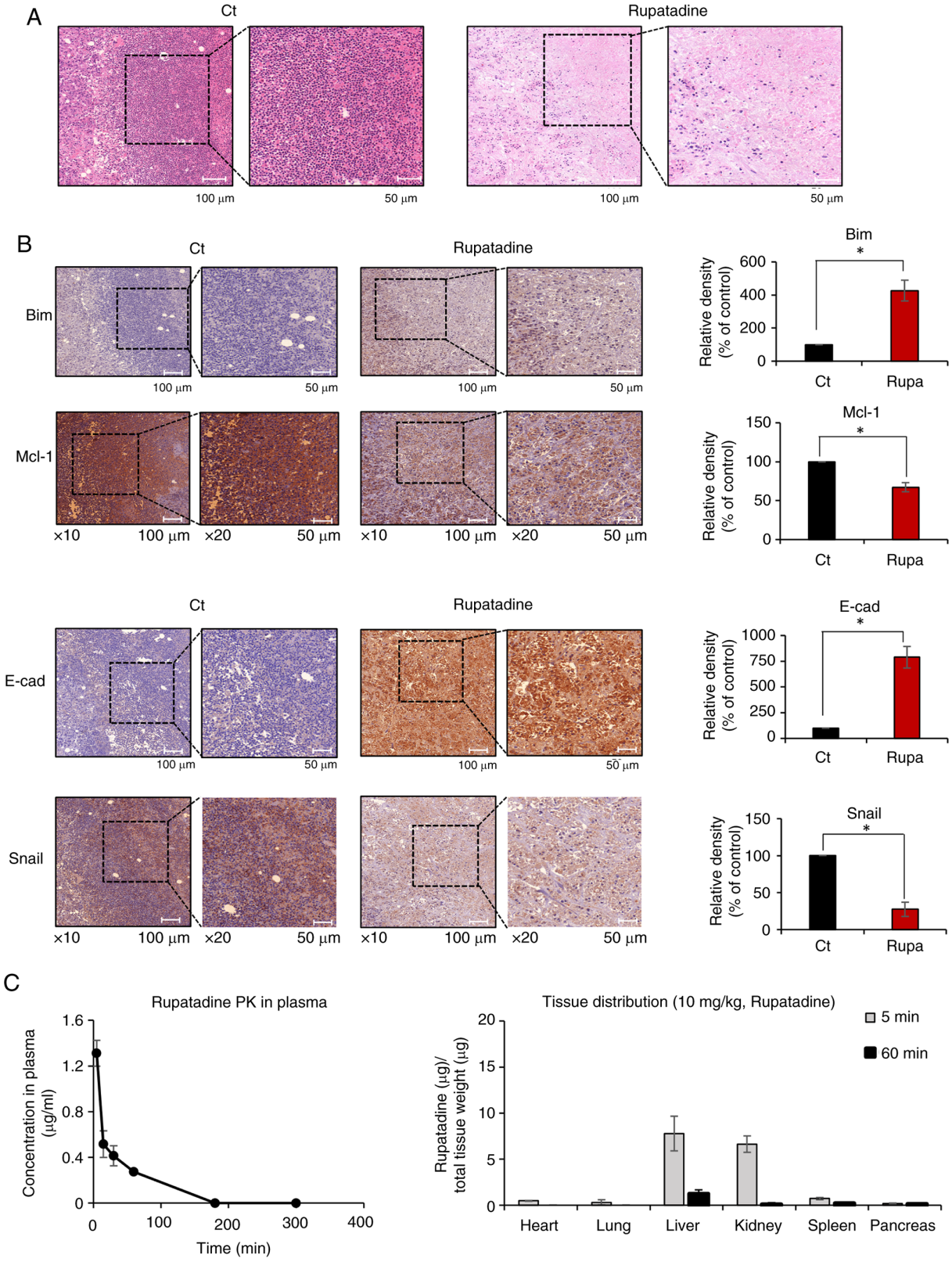

Figure 6. Impact of rupatadine on histological changes in a pancreatic cancer xenograft mouse model. (A) H&E staining of excised tumor tissues, demonstrating a notable reduction in tumor cell density in the rupatadine-treated group. (B) Immunohistochemical analysis for the markers of apoptosis and EMT. Rupatadine-treated group exhibited increased immunoreactivity for the pro-apoptotic marker BIM and decreased expression of the anti-apoptotic marker Mcl-1. In addition, the rupatadine-treated group exhibited decreased immunoreactivity for the epithelial marker E-cadherin and decreased expression of the mesenchymal marker Snail. For 10x magnification, the scale bar is 100 μm; for 20x magnification, the scale bar is 50 μm. (C) Pharmacokinetic and tissue distribution analysis of rupatadine *in vivo*. (Left) Plasma concentration-time curve of rupatadine following intravenous administration (10 mg/kg) in mice. Rupatadine was rapidly cleared from plasma, with undetectable levels beyond 180 min. (Right) Tissue distribution of rupatadine at 5 and 60 min post-injection, showing predominant accumulation in the liver and kidneys at early time points, with minimal retention after 60 min. Values are presented as mean ± SD of three independent experiments. Percentages of immunoreactive areas were measured using Image J (National Institute of Health) and expressed as relative values to those in control tissues. *P<0.05 vs. the control. H&E, hematoxylin and eosin staining; EMT, epithelial-mesenchymal transition; BIM, Bcl-2 interacting mediator of cell death; Ct, control; Mcl-1, Myeloid cell leukemia-1; E-cad, E-cadherin; Rupa, Rupatadine.

functions, likely contribute to its efficacy in inhibiting EMT processes in pancreatic cancer cells.

This study confirms that rupatadine's anticancer efficacy is primarily derived from its dual action of inhibiting EMT and promoting apoptosis. In addition, this study has shown that Rupatadine can have anticancer effect by inhibiting the TGFβ1 signaling pathway which promotes cancer cell invasion, angiogenesis, and immune evasion within the tumor microenvironment, facilitating tumor progression and metastasis. The inhibitory effects of Rupatadine on the TGF-β signaling pathway have been demonstrated in numerous previous studies (10-13). Especially, Didamoony *et al* (11) delineates that Rupatadine mediates its anticancer efficacy through the inhibition of the TGF-β1 pathway, potentially by modulating associated pathways such as PAF, NF-κB, and p65. Furthermore, Rupatadine's anticancer effects can be partly linked to its role in causing mitochondrial and lysosomal damage (9). As a cationic amphiphilic drug, Rupatadine can easily enter cells and accumulate in lysosomes, the cell's waste disposal system. This leads to the disruption of the lysosomal membrane, releasing enzymes that trigger cell death.

Although the AsPC-1 and MIA PaCa-2 cell lines used in this study were obtained from an authenticated source, additional in-house authentication and mycoplasma testing were not performed prior to the experiments. While the passage numbers were kept relatively low (passage 11 for AsPC-1 and passage 13 for MIA PaCa-2), we acknowledge that prolonged culture and high passage numbers may contribute to genetic and phenotypic variability, which could influence experimental outcomes. Future studies should consider regular authentication to ensure reproducibility and minimize variability associated with cell culture conditions.

In conclusion, this study highlights rupatadine's anticancer effects in pancreatic cancer models. The *in vitro* results demonstrated rupatadine's capacity to suppress EMT and enhance apoptosis in pancreatic cancer cells. In a pancreatic cancer xenograft mouse model, intravenous administration of rupatadine led to a significant tumor weight reduction. Further analysis of the excised tumor tissue from this model reinforced the observation that rupatadine's anticancer efficacy largely stems from its dual action in inhibiting EMT and facilitating apoptosis. Future studies are needed to elucidate the precise mechanisms underlying these effects. In addition, expanding the panel of pancreatic cancer cell lines in future experiments will help validate the generalizability of our findings and further support the clinical relevance of rupatadine. Moreover, while the present study focused on monotherapy, future investigations will evaluate the combinatorial potential of rupatadine with established chemotherapeutic agents and targeted therapies to better reflect clinical treatment strategies. Overall, rupatadine can be considered as a promising candidate for pancreatic cancer therapy, offering a unique mechanism of action that could synergize effectively with existing treatment modalities in a combination therapy approach.

Acknowledgements

The authors would like to thank Ms Jeong-Yeon Seo (Translational Research Team, Surginex Co., Ltd., Seoul, South Korea) for manuscript processing and Ms Jennifer Lee (Translational Research Team, Surginex Co., Ltd., Seoul, South Korea) for their contributions to the illustrations.

Funding

This work was supported by the financial support of the Catholic Medical Center Research Foundation made in the program year of 2021.

Availability of data and materials

The data generated in the present study may be requested from the corresponding author.

Authors' contributions

SJK conceptualized the study and was project administrator. BJC analyzed and interpreted the data and wrote the original draft. BJC, HJC, DL, JHP and THH performed the animal experiments. HJJ, GHJ and OHK performed the *in vitro* experiments. All authors have read and approved the final manuscript. SJK and BJC confirm the authenticity of all the raw data.

Ethics approval and consent to participate

Our animal experiments were approved by the Institutional Animal Care and Use Committee of the Catholic University of Korea (approval no. CUMC-2022-0014-01) and were conducted in accordance with institutional and national guidelines for the care and use of laboratory animals.

Patient consent for publication

Not applicable.

Competing interests

The authors declare that they have no competing interests.

References

1. Jiang Z, Zheng X, Li M and Liu M: Improving the prognosis of pancreatic cancer: Insights from epidemiology, genomic alterations, and therapeutic challenges. Front Med 17: 1135-1169, 2023.
2. Rahib L, Wehner MR, Matrisian LM and Nead KT: Estimated projection of US cancer incidence and death to 2040. JAMA Netw Open 4: e214708, 2021.
3. Siegel RL, Miller KD, Fuchs HE and Jemal A: Cancer statistics, 2021. CA Cancer J Clin 71: 7-33, 2021.
4. Mizrahi JD, Surana R, Valle JW and Shroff RT: Pancreatic cancer. Lancet 395: 2008-2020, 2020.
5. Park W, Chawla A and O'Reilly EM: Pancreatic cancer: A review. JAMA 326: 851-862, 2021.
6. Awais N, Satnarine T, Ahmed A, Haq A, Patel D, Hernandez GN, Seffah KD, Zaman MA and Khan S: A systematic review of chemotherapeutic regimens used in pancreatic cancer. Cureus 15: e46630, 2023.
7. Deuster E, Hysenaj I, Kahaly M, Schmoeckel E, Mayr D, Beyer S, Kolben T, Hester A, Kraus F, Chelariu-Raicu A, *et al*: The platelet-activating factor receptor's association with the outcome of ovarian cancer patients and its experimental inhibition by rupatadine. Cells 10: 2337, 2021.
8. Faustino-Rocha AI, Ferreira R, Gama A, Oliveira PA and Ginja M: Antihistamines as promising drugs in cancer therapy. Life Sci 172: 27-41, 2017.

9. Cornet-Masana JM, Banus-Mulet A, Carbo JM, Torrente MA, Guijarro F, Cuesta-Casanovas L, Esteve J and Risueno RM: Dual lysosomal-mitochondrial targeting by antihistamines to eradicate leukaemic cells. EBioMedicine 47: 221-234, 2019.
10. Ahmed LA, Mohamed AF, Abd El-Haleim EA and El-Tanbouly DM: Boosting Akt pathway by rupatadine modulates Th17/Tregs balance for attenuation of isoproterenol-induced heart failure in rats. Front Pharmacol 12: 651150, 2021.
11. Didamoony MA, Atwa AM and Ahmed LA: A novel mechanistic approach for the anti-fibrotic potential of rupatadine in rat liver via amendment of PAF/NF-kB p65/TGF-beta1 and hedgehog/HIF-1alpha/VEGF trajectories. Inflammopharmacology 31: 845-858, 2023.
12. Didamoony MA, Atwa AM and Ahmed LA: Modulatory effect of rupatadine on mesenchymal stem cell-derived exosomes in hepatic fibrosis in rats: A potential role for miR-200a. Life Sci 324: 121710, 2023.
13. Lv XX, Wang XX, Li K, Wang ZY, Li Z, Lv Q, Fu XM and Hu ZW: Rupatadine protects against pulmonary fibrosis by attenuating PAF-mediated senescence in rodents. PLoS One 8: e68631, 2013.
14. Yuan W, Fang W, Zhang R, Lyu H, Xiao S, Guo D, Ali DW, Michalak M, Chen XZ, Zhou C, *et al*: Therapeutic strategies targeting AMPK-dependent autophagy in cancer cells. Biochim Biophys Acta Mol Cell Res 1870: 119537, 2023.
15. Paunovic V, Kosic M, Misirkic-Marjanovic M, Trajkovic V and Harhaji-Trajkovic L: Dual targeting of tumor cell energy metabolism and lysosomes as an anticancer strategy. Biochim Biophys Acta Mol Cell Res 1868: 118944, 2021.
16. Debnath J, Gammoh N and Ryan KM: Autophagy and autophagy-related pathways in cancer. Nat Rev Mol Cell Biol 24: 560-575, 2023.
17. Bhagya N and Chandrashekar KR: Liposome encapsulated anticancer drugs on autophagy in cancer cells - Current and future perspective. Int J Pharm 642: 123105, 2023.